Sustainable Energy & Fuels

Facile Synthesis and Characterization of γ-Al2O3 Loaded on Reduced Graphene Oxide Hybrids for Electrochemical Reduction of CO2

Journal:	*Sustainable Energy & Fuels*
Manuscript ID	SE-ART-07-2022-000953.R1
Article Type:	Paper
Date Submitted by the Author:	28-Sep-2022
Complete List of Authors:	Mulik, Balaji; Dr Babasaheb Ambedkar Marathwada University, Department of Chemistry Bankar, Balasaheb; Central Salt and Marine Chemicals Research Institute CSIR, Inorganic Materials and Catalysis Munde, Ajay; Dr Babasaheb Ambedkar Marathwada University, Chemistry Biradar, Ankush; CSIR-Central Salt and Marine Chemicals Research Institute, Inorganic Materials and Catalysis Asefa, Tewodros; Rutgers The State University of New Jersey, Department of Chemistry and Chemical Biology; Rutgers The State University of New Jersey, Department of Chemical and Biochemical Engineering Sathe, Bhaskar; Dr Babasaheb Ambedkar Marathwada University, Chemistry

ARTICLE

Facile Synthesis and Characterization of γ-Al_2O_3 Loaded on Reduced Graphene Oxide for Electrochemical Reduction of CO_2

Received 00th January 20xx,
Accepted 00th January 20xx

DOI: 10.1039/x0xx00000x

Balaji B. Mulik,[a,d] Balasaheb D. Bankar,[b] Ajay V. Munde,[a] Ankush V. Biradar,[b]* Tewodros Asefa[e,f]* and Bhaskar R. Sathe[a,c]*

Electrocatalytic reduction of CO_2 to valuable organic compounds and fuels using energy efficient techniques is presently of great importance. In this work, we show the synthesis of Al_2O_3-decorated reduced graphene oxide (rGO) electrocatalysts and their catalytic properties for the conversion of CO_2 into formate. These hybrid nanostructured materials are prepared using chemical synthesis, followed by chemical vapor deposition. The materials are characterized by X-ray diffraction and Raman spectroscopy, and the results confirm the formation of γ-Al_2O_3 on defect-rich rGO. Transmission electron microscope images reveal the formation of γ- Al_2O_3 with particle sizes of 8±0.3 nm on rGO sheets that are ~100 x 100 nm in length and width and that are composed of a few-layers of graphene. X-ray photoelectron spectroscopy confirms the presence of Al-O, C-C and C-O bonds in the material. The amount of Al is ~2.8 %, as determined by inductively coupled plasma-mass spectrometry (ICP-MS). The material catalyzes the electrochemical reduction of CO_2 at a potential of -0.434 V vs. RHE in 0.5 M $KHCO_3$ solution, which is used as an electrolyte. The potential dependent bulk electrolysis shows that the reduction product is formate, which forms with a Faradaic efficiency (FE) of 31.90, 37.25, 42.50, 55.10 and 91.20% at potentials of -0.434, -0.534, -0.634, -0.734 and -0.934 V vs. RHE, respectively. Based on these findings, these noble metal-free electrocatalysts may find industrial applications to convert CO_2 into valuable chemicals, thereby to mitigate CO_2-related global warming issues.

Introduction

Energy crises and global warming are currently among the major obstacles to sustainable societal development worldwide. The projected total energy demand in 2050 is expected to be two-fold higher than what was in 2019. Although fossil fuels, which include coal, petroleum and natural gas are relatively inexpensive and energy-dense natural resources, their incessant consumption is gradually depleting these natural energy resources.[1] Moreover, their use has been raising the amount of carbon dioxide (CO_2) in the atmosphere and causing grave greenhouse effect and global warming. Thus, it is important to develop new and alternative ways to generate energy and thereby lower fossil fuel use.[2]

The possible ways to do so includes the transformation of CO_2 into value-added chemicals and synthetic fuels using biocatalysts,[3] chemical and thermal transformation methods,[4] CO_2 hydrogenation under high pressure and using various reagents,[5] and photocatalytic and electrocatalytic hydrogenation reactions.[6] Many of these methods, which can recycle CO_2, involve CO_2 adsorption, activation and transformation steps. However, not only they require enormous amounts of thermal energy, high H_2 pressure or chemical reagents to activate the stable CO_2 molecule but they also unfortunately take place with low transformation rates. Electrocatalytic reduction of CO_2, in contrast, has the following three major advantages: (i) It can be applied directly for practical use under thermodynamically favorable (electron and proton transfer) experimental conditions; (ii) It is more environmentally friendly; and (iii) It allows for product selectivity by applying the right potential, temperature, solvent, electrolyte or electrocatalyst. Moreover, the potential needed for the electrocatalytic transformation of CO_2 can be derived from non-fossil fuels-based energy sources, such as wind power, solar energy, and hydroelectricity.[7]

The electrochemical reduction of CO_2 can give various products or a mixture of products, including formate ($HCOO^-$), carbon monoxide (CO), methanol (CH_3OH), and methane (CH_4), depending on the number of electrons and protons transferred at the electrified interface during the reaction.[8] For example, Hori *et al.* showed that the Faradaic efficiency (FE) of CO_2 reduction, which is a measure of electrocatalytic activity) and

[a] Department of Chemistry Dr. Babasaheb Ambedkar Marathwada University, Aurangabad 431004, Maharashtra, India
[b] Inorganic Material and Catalysis Division, CSIR-Central Salt and Marine Chemicals Research Institute, Bhavnagar 364002, Gujarat, India
[c] Department of Nanotechnology, Dr. Babasaheb Ambedkar Marathwada University, Aurangabad 431004, Maharashtra, India
[d] University Department of Basic and Applied Science (Chemistry), MGM University, Aurangabad 431003, Maharashtra, India
[e] Department of Chemistry and Chemical Biology Rutgers, The State University of New Jersey, 610 Taylor Road, Piscataway, NJ, 08854, USA
[f] Department of Chemical and Biochemical Engineering, Rutgers, The State University of New Jersey, 98 Brett Road, Piscataway, NJ, 08854, USA
† Footnotes relating to the title and/or authors should appear here.
tasefa@chem.rutgers.edu; ankush@csmcri.res.in, bhaskarsathe@gmail.com

the product selectivity of the electrocatalytic reaction, were highly dependent on the type of electrolyte used, the types and stability of intermediate species formed in the reaction, and the nature of the catalyst used.[9] Although noble metals such as Rh and Pd can electrocatalyze CO_2 reduction,[10] these catalysts have low FE values toward desirable products because of their inherent ability to catalyze also the competitive hydrogen evolution reaction (HER) at nearly similar cathodic potentials.

The activity of solid-state electrocatalysts depends considerably on the atomic size, oxidation state, and chemical nature of the atoms involved. Nanostructured electrocatalysts possess a large surface area-to-volume ratio, many surface atoms with large surface energy, high reactivity, and tunable spatial/quantum confinement effects. Due to these properties, nanomaterials not only display distinct chemical, physical, and surface properties compared to their bulk/molecular counterparts but are also more active as electrocatalysts.[11] Recently, an excellent review on various nanostructured metals, metal oxides and carbon materials that show good catalytic activities for electrochemical reduction of CO_2, their advantages for electrocatalysis, and the different factors affecting their activities and FE values to the different products forming over them was recently published by Hou *et al*.[12]

Formic acid and formate, which are among possible CO_2 reduction products, are widely used for agricultural and pharmaceutical applications, in organic synthesis, and in the food and textile industries. They can also serve as an easier and safer medium to store and deliver H_2 generated by water splitting reactions for fuel cells.[13] Both of them can be accessed *via* electrochemical reduction of CO_2 that involves 2-electron and 2-proton transfer processes and $CO_2^{\cdot-}$ intermediate at the electrified interfaces.[14,15] However, getting exclusively only these products with CO_2 electroreduction is not straightforward. Several transition metal-based electrocatalysts have been investigated for the selective conversion of CO_2 into formate. For example, White and Bocarsly reported that indium oxide, indium hydroxide and metallic indium nanoparticles could catalyze the electrochemical reductive conversion of CO_2 into formate.[16] Due to their higher surface area and density of surface exposed active sites, such nanoscale materials unsurprisingly show significantly enhanced activity compared to their bulk counterparts. Chen and Kanan studied the electrochemical reduction of CO_2 on thin films of Sn/SnO_x electrodes in aqueous $NaHCO_3$ supporting electrolyte.[17] These SnO_x thin film-based systems displayed 8-fold higher fractional current density and nearly 4-fold greater Faradaic efficiency (FE) for electrocatalytic hydrogenation of CO_2 as compared with Sn film electrode. While other nanostructured systems, such as Hg-based amalgam, Sn@Bi nanoparticles[17,18] and Pb and polytetrafluoroethylene electrode[19,20] have been reported for CO_2 reduction and formate formation, many of them suffer from surface poisoning, higher overpotentials, etc.

Meanwhile, two-dimensional (2D) materials have recently attracted much attention because they enable the dispersion of metal nanoparticles and prevent their aggregation, giving stable heterogeneous nanocatalysts. Graphene oxide (GO) is a notable such 2D material that has bonds composed of sp^2 and sp^3 hybridized carbon atoms and a planar network with high mobility of π-electrons available for binding other agents. GO also contains oxygen-based functional groups such as hydroxyls, epoxides and carbonyl on its surfaces, and these groups make GO hydrophilic and dispersible in water.[21] GO has been used as a support material for catalysis and electrocatalysis applications, including electrochemical hydrogenation of CO_2.[22-28] For example, Fischer *et al.* used graphene nanoribbons as support materials for Au nanoparticles, and the resulting materials were found to electrochemically catalyze the hydrogenation of CO_2 to CO with 90% FE at -0.2V vs. RHE.[29] Zygmunt*et al.* synthesized ZnO-supported graphene for activation of CO_2 and studied the effect of the support material on the rate of CO_2 reduction.[30] Meyer *et al.* reported graphene-supported Sn nanoparticles that could electrochemically reduce CO_2 to formate product in aqueous $NaHCO_3$ electrolyte with a 93% FE.[31] These materials showed high catalytic activity due to the synergetic effects and strong interaction between their constituents. Kimura *et al*. prepared different Cu-based gas diffusion electrodes using ZnO, ZrO_2, TiO_2, Al_2O_3, and Nb_2O_5 as support materials and found that the products forming from the reactions would depend on the types of metal oxide support materials used.[32]

So far, only very few studies have been reported on Al-based electrocatalysts for the electrochemical conversion of CO_2 into useful products. Biswal*et al.* reported *γ*-Al_2O_3- and ZSM-5-supported Sn for electrocatalytic hydrogenation of CO_2 to methane.[33] Notably, they studied 20 wt% Sn electrocatalyst loaded on *γ*-Al_2O_3 and ZSM-5, and they found that the porous walls of *γ*-Al_2O_3 would give more Faradic current with high yield of methane than those of ZSM-5. Al_2O_3 could do so because it enabled Sn to disperse better, forming less agglomerates, than ZSM-5. Very recently, the stability of γ-Al_2O_3-supported SnO_2 during the electrochemical reduction of CO_2 to formate was reported.[34] The support material (i.e., γ-Al_2O_3) prevented the etching of Sn, increasing the stability of the supported SnO_2 nanoparticles and helping them retain their size, morphology and crystallinity. However, the electrochemical activity, selectivity and FE (65%) of *γ*-Al_2O_3-supported SnO_2 electrocatalyst are still low, even after 152 h-long electrolysis.

Herein, we report the synthesis and characterization of Al_2O_3-decorated reduced graphene oxide (Al_2O_3-rGO) via chemical vapor deposition (CVD). We also show that this hybrid material shows electrocatalytic activity for the hydrogenation of CO_2 (CO_2 reduction) in aqueous $KHCO_3$ electrolyte. The product of the reaction is formate, as confirmed with HPLC, and it forms with FE values of 31.90, 55.10 and 91.20% at potentials of -0.434 V, -0.734 V and -0.934 V vs. RHE, respectively.

Experimental

Chemicals

Aluminium chloride ($AlCl_3$) (Sigma-Aldrich), graphite powder (99.99%, Alfa-Aesar), sulphuric acid (98% Alfa-Aesar), nitric acid (78% Alfa-Aesar), potassium bicarbonate (Sigma-Aldrich), acetone (99.99% Alfa-Aesar), and CO_2 gas (99.99%) and

hydrazine hydrate (N_2H_4) (99.99%) (Vijay Scientific Ltd., India) were procured and used as received. Deionized water was used for all synthetic work and electrochemical studies.

Synthesis of GO, reduced GO (rGO) and Al_2O_3-rGO

GO was synthesized from graphite powder using the modified Hummer's method.[21-28] Briefly, in a round-bottom flask, 0.5 g of graphite powder was mixed with 100 mL of acidic solution containing concentrated HNO_3 and H_2SO_4 (3:1), and the mixture was stirred in an ice bath for 45 min. The dispersion was then sonicated for 3 h in an ultra-sonication bath. It was subsequently refluxed for 24 h. It was then diluted with distilled water and filtered. The solid product was redispersed in THF to remove unreacted graphite. It was filtered again and washed with acetone. The precipitate was dried in oven at a temperature of 60 °C for 2 h to remove the solvent and any other volatile substances. Then, 0.5 g of the product, which is GO, was taken and mixed with hydrazine hydrate (2-5 mL), and the mixture was stirred for 2 h. The dispersion was filtered, and the solid material was washed copiously with deionized water and then ethanol. It was dried giving rGO. The rGO was used to synthesize the nanocomposite materials below.

To synthesize Al_2O_3-rGO, first rGO and $AlCl_3$ were mixed in 1:1 ratio by weight using mortar and pestle. The mixture was kept in a CVD furnace and treated at 600 °C in Ar atmosphere for 2 h, followed by in H_2 atmosphere for 3 h. The formation of Al_2O_3-rGO nanocomposite material was confirmed by various physicochemical characterization techniques. The synthetic procedure leading to Al_2O_3-rGO, along with the electrocatalytic evaluation of the material, is schematically illustrated in Scheme 1.

Fabrication of Al_2O_3, rGO and Al_2O_3-rGO-modified electrode and electrocatalytic studies

All electrochemical studies were performed using a CHI-660E potentiostat (CH-instrument, USA) and a three-electrode cell comprising a saturated calomel (SCE) reference electrode, a Pt wire counter electrode, and a working electrode. The working electrode is comprised of a glassy carbon (GC) with a diameter of 3 mm that contains each catalyst. Before depositing the catalyst on it, the GC electrode was cleaned by polishing it with 1.0, 0.3 and 0.05 µm-sized Al_2O_3 powders, followed by washing it with water and methanol to remove inorganic and organic impurities, respectively. A calculated amount (0.01 mg) of Al_2O_3, rGO or Al_2O_3-rGO in 1 mL isopropanol was sonicated for 40 min. The catalyst ink was then drop-casted on the active area of the GC. The resulting Al_2O_3, rGO and Al_2O_3-rGO-modified GC working electrode was used for electrochemical and electrocatalytic studies. As an electrolyte, an aqueous solution of $KHCO_3$ (0.5 M) was used. N_2 gas was bubbled in the aqueous electrolyte for 30 min to remove dissolved O_2, before bubbling CO_2 gas for 40 min to saturate it with CO_2. The electrochemical data collected using SCE were converted into the reversible hydrogen electrode (RHE) using the following equation (Eq. 1).

$$V_{RHE} = V_{SCE} + 0.2412 + 0.059pH \quad \text{---------- Eq. 1}$$

The pH here, which refers to that of the electrolyte after CO_2 saturation, is 7.2.

Characterization

X-ray diffraction (XRD) patterns of the materials were obtained using a Rigaku-Ultima IV fully automatic high-resolution X-ray diffractometer equipped with X-ray generator operating at 40 kV and 40 mA. The measurements were performed in a step of 0.01° (2θ) at room temperature. Raman spectroscopic analysis of the materials was performed with a Raman optics that is equipped with a microscope (Seki Technotron Corporation) and operating with 532 nm laser. X-ray photoelectron spectroscopy (XPS) was performed with SPECS HSA-3500 instrument that is operating with a monochromatic Al Kα X-ray radiation source and that has a hemispherical analyzer. The XPS results were used to investigate the elemental states of the samples. The morphologies and sizes of the as-prepared hybrid materials were examined by transmission electron microscopy (TEM). The amount of Al in Al_2O_3-rGO was determined by inductively coupled plasma-mass spectrometry (ICP-MS). The samples for it were prepared via digestion of 10 mg of materials with aqua regia (HCl/HNO_3). The data was used to calculate the elemental composition of the materials.

Results and discussion

Al_2O_3-rGO is synthesized with a two-step synthetic procedure involving the chemical immobilization of Al^{3+} ions into rGO, followed by heat treatment/chemical vapor deposition (CVD), as illustrated in Scheme 1. The material is characterized by various methods. First, the XRD patterns of Al_2O_3-rGO and the parent material GO are obtained to compare the phases and crystallinity of the components in them. The XRD pattern of rGO (**Figure 1,a**) shows the typical diffraction peaks of the (002), (101) and (110) planes of graphitic carbon.[35] While the XRD pattern of Al_2O_3-rGO shows similar peaks, the peaks are shifted to higher angles (by 2θ of ca. 0.30°). It also shows additional Bragg peaks corresponding to the (200), (222), (400) and (440) planes of γ-phase of Al_2O_3, in fair agreement with what is reported for this material in the literature. Not surprisingly, the peaks in the XRD patterns appear broader most likely due to their small particle sizes.[36]

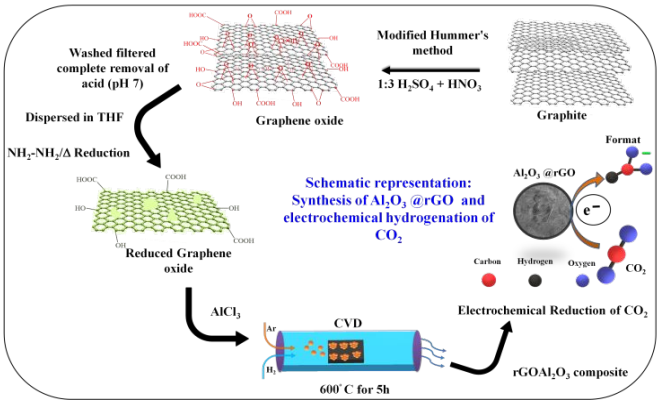

Scheme 1. Illustration of the synthetic procedure used to produce tunable Al_2O_3-rGO electrocatalyst for electrochemical reduction of CO_2 to formate. The synthesis involves the preparation of GO, followed by reduction of its surface oxides to form rGO, and finally the decoration of the surfaces of rGO with Al_2O_3.

To determine the degree of defect sites in the graphene structures of rGO, before and after decoration with Al_2O_3, the Raman spectra of rGO and Al_2O_3-rGO are obtained **Figure 1(b)**. Their superimposed spectra show weak bands at ~110, ~189 and ~274 cm^{-1} that can be attributed to Al_2O_3. The peaks are weak because Al_2O_3 is present in nanosized form or in small amount. The peak observed at ~1345 cm^{-1} in the spectra is due to a D-band, indicating the presence of some disordered structure in the graphene sheet. The peak observed at ~1571 cm^{-1} is a G-band corresponding to graphitic structure in rGO. The ratio of intensity of the two bands (I_D/I_G) for rGO is 0.68. The one for Al_2O_3-rGO is much higher (0.91). This means the I_D/I_G ratio increases after decoration of rGO by Al_2O_3 indicating the formation of more defect structures in it compared with the pristine one. Moreover, a shift to negative values (by ca. 5.9 cm^{-1}) of both D and G bands of Al_2O_3-rGO compared with those of rGO might be due to the change in the electronic structure of rGO after its decoration with Al_2O_3 nanoparticles.[37]

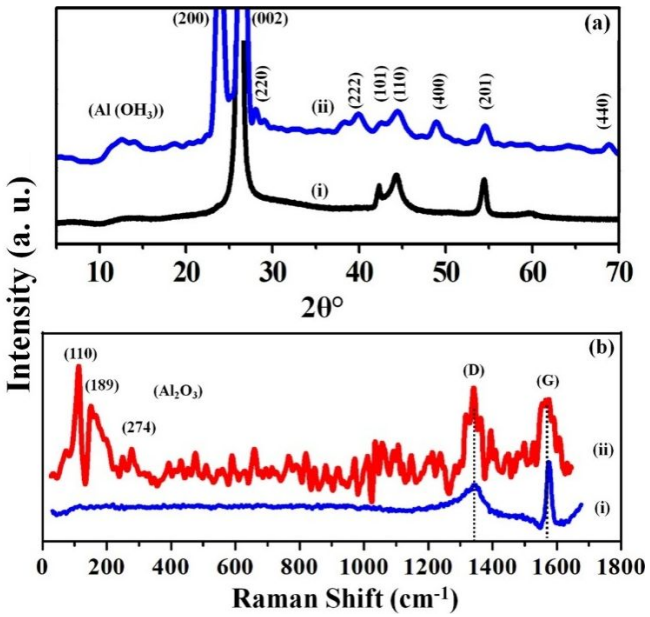

Figure 1. Superimposed (a) XRD patterns of (i) rGO and (ii) Al_2O_3-rGO. The results indicate that the latter has γ phase Al_2O_3. (b) Raman spectra of (i) rGO and (ii) Al_2O_3-rGO. The ratio of intensities of the peaks associated with the D and G bands (I_D/I_G) of rGO is 0.68, and the one for Al_2O_3-rGO is 0.91 (or five-time higher after Al_2O_3 nanoparticles are incorporated in rGO).

Next, the morphologies and structures of the as-synthesized nanocomposite materials are studied using TEM. The result is shown in Figure 2. The image shows that rGO sheet has a size of ca. ~100 nm x 100 nm and is decorated with Al_2O_3. Al_2O_3 particles are quasi-spherical in shape and have an average size of 8±0.3 nm (see the particle size distribution curve shown in **Figure S1** in SI).

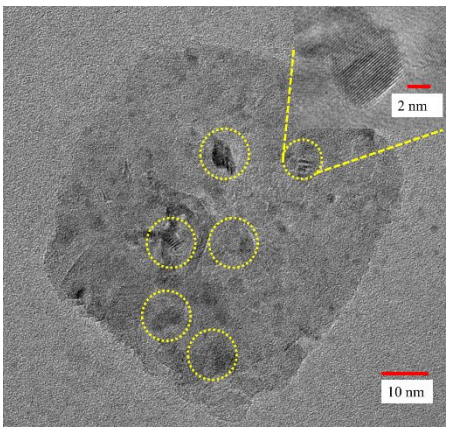

Figure 2. Transmission electron microscopy (TEM) image of Al_2O_3-rGO. The average size of Al_2O_3 particles on the 100 nm-size nanosheet of rGOis 8±0.3 nm. The inset shows a high-resolution TEM (HRTEM) of an individual Al_2O_3 nanoparticle on rGO nanosheet.

The as-synthesized Al_2O_3-rGO is then characterized by XPS (**Figure 3)**. The full survey XPS spectrum shows the presence of C, O and Al (see **Figure 3a**).The deconvolution of C 1s peak gives four bands indicating the presence of different oxidized carbon species and defect sites in the material (**Figure 3b**). The intense peak at 284.8 eV represents asymmetric C-C groups, the peak at 286.01 eV is related to C-O-C groups, the one at 287.2 eV can be ascribed to C=O and the peak at 288.8 eV is associated with the atoms in C=C bonds.[38] The XPS spectrum of Al of Al_2O_3-rGO is depicted in **Figure 3c** and exhibits two peaks at 74.4 eV and 75.20 eV associated with $2p_{3/2}$ and $2p_{1/2}$ of Al in +3 oxidation state, which corresponds to Al_2O_3. Meanwhile, the peak observed at a binding energy of 73.3 eV corresponds to metallic Al.[39] The deconvoluted spectrum of the core level O 1s is shown in **Figure 3d**. It shows a peak at 530.5 eV, which corresponds to Al-O bond; a second peaks at 531.1 eV, which is associated with O-H functional groups; and a third one at a 533.1 eV, which is due to C=O species.[40] The XPS results collectively confirm that the composite material has Al_2O_3 and rGO. The presence of these two materials together is found to impart synergetic electrocatalytic effects to effectively drive CO_2 reduction reactions at the electrode/electrolyte interface to specific intermediates such as *OCHO species (*vide infra*).

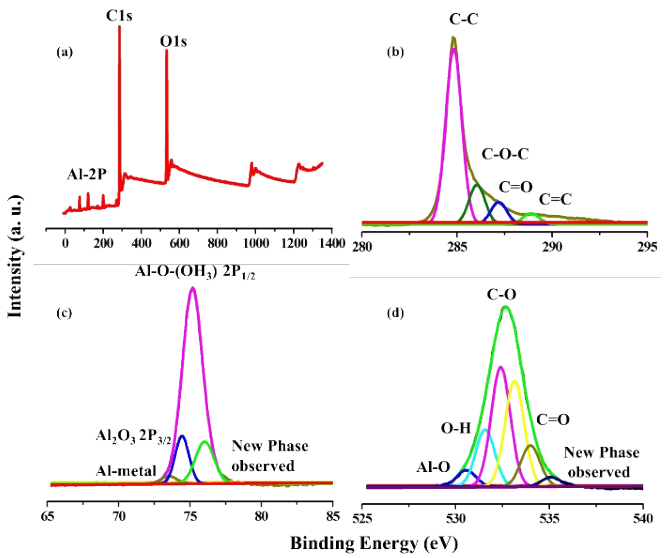

Figure 3. X-ray photoelectron spectra (XPS) of Al_2O_3-rGO. (a) Full XPS survey spectrum showing signals corresponding to Al, O and C. (b) XPS spectra C1s core electron deconvoluted into four different species (C-C, C-O-C, C=O and C=C). (c) XPS peaks of Al 2p core-shell levels ($2p^{3/2}$ and $2p^{1/2}$). (d) XPS O1s peak deconvoluted into peaks corresponding to Al-O, O-H, and C-O species.

Moreover, the amount of Al in Al_2O_3-rGO nanocomposite material, which is determined by ICP-MS, is ~2.8 %. The data observed has been incorporated in **Figure S2** in the SI.

Next, cathodic current versus potential curves are obtained for the catalyst and the relevant control materials. The studies are done using 0.5 M $KHCO_3$ saturated with N_2 or CO_2 gas as an electrolyte at a scan rate of 50 mV s^{-1} and in the potential window of 0.668 to -0.934V vs. RHE. The studies include cyclic voltammetry (CV), linear sweep voltammetry (LSV), chronoamperometric measurements (i-t) and electrochemical impedance spectroscopy (EIS). For a better comparison, the LSV curves of Al_2O_3-rGO obtained in saturated N_2 gas and in CO_2 gas are overlaid in **Figure 4a**, (i) and (ii). The LSV curves, shown in **Figure 4a**, reveal that the electrochemical reduction of CO_2 over Al_2O_3-rGO takes place at an onset potential of -0.434 V vs. RHE. This value is lower as compared with those of the other electrocatalysts, namely, Al_2O_3 NPs, rGO, and bare GC, denoted in **Figure 4a**, as (iii), (iv) and (v). Besides, the current density obtained for the former is higher. The higher current density and lower onset potential obtained in CO_2 environment for Al_2O_3-rGO indicate its viability for efficient electrochemical reduction of CO_2.[41]

Electrochemical impedance spectra (EIS) and Nyquist plots for the materials are then obtained. Impedance measurements indirectly signify the kinetics of electrochemical oxidation-reduction reactions at the electrode/electrolyte interfaces and help to determine the electro activity of materials.[42] In Nyquist plots, smaller semicircles indicate easier or more feasible electron transfer processes, relating to the resistance in the Ohm's law.

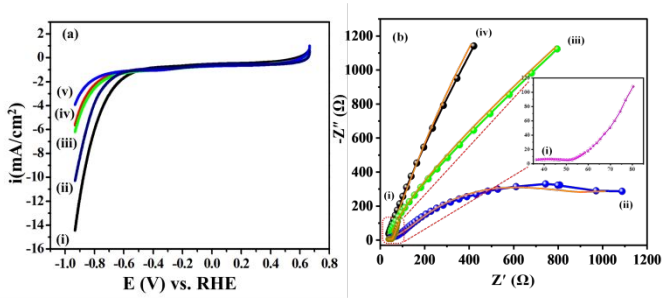

Figure 4 (a) Superimposed LSV curves obtained at a scan rate of 50 mV s^{-1} for electrochemical reduction of CO_2. Prior to the experiments, the electrolyte is bubbled with N_2 gas (for 30 min) to remove dissolved O_2, followed by CO_2 gas (for 40 min) to saturate it with CO_2, except for the control experiment in (ii), in which case only N_2 gas was bubbled. The experiments are done over (i) Al_2O_3-rGO in $KHCO_3$ solution (0.5 M) bubbled with N_2 and then CO_2, (ii) Al_2O_3-rGO in $KHCO_3$ solution (0.5 M) saturated only with N_2 gas, (iii) Al_2O_3 bubbled with N_2 and then CO_2, (iv) rGO saturated with N_2 and then CO_2, and (v) bare GC in 0.5 M $KHCO_3$ solution bubbled with N_2 and then CO_2. (b) Nyquist plots for CO_2 reduction at an applied potential of -0.848 V vs. RHE over (i) Al_2O_3-rGO hybrid nanocomposite bubbled with N_2 then CO_2 (value Al_2O_3-rGO hybrid nanocomposite) (ii) Al_2O_3 bubbled with N_2 then CO_2, (iii) rGO bubbled with N_2 gas then CO_2, and (iv) bare GC in 0.5 M $KHCO_3$ bubbled with N_2 and then CO_2.

Figure 4b shows the EIS plots obtained at an applied potential of -0.848 V vs. RHE for (i) Al_2O_3-rGO hybrid nanocomposite material, (ii) Al_2O_3, (iii) rGO, and (iv) bare GC in $KHCO_3$ electrolyte bubbled with N_2, followed with CO_2. The results indicate that Al_2O_3-rGO has the lowest resistivity (with a value of R_{ct} = 21.5Ω) compared with Al_2O_3 (with R_{ct} = 26.1 Ω), rGO (with R_{ct} = 28.6Ω) and bare GC (with R_{ct} = 58.3 Ω). Furthermore, **Figure S3** in SI shows an equivalence circuit model and corresponding evaluated electrochemical resistance values observed are for (a) bare GC electrode @9.62 Ω, (b) Al_2O_3 NPs modified GC electrode @8.3 Ω, (c) rGO modified GC electrode @5.46 Ω and (d) Al_2O_3-rGO modified GC electrode @2.73 Ω hybrid nanocomposite with EIS plot. These results indicate that Al_2O_3-rGO has a relatively greater conductivity and ability to transfer electron during electrocatalytic CO_2 reduction.

To examine the stability and the potential of Al_2O_3-rGO catalyst to reduce CO_2 on a large scale, chronoamperometric (i-t) measurements at different applied potentials using $KHCO_3$ solution (0.5 M) as a supporting electrolyte are carried out. The results are displayed in **Figure 5(a)**. In the experiments, the potential is kept constant for a particular period of time. The changes observed in the electrocatalytic reduction reaction of CO_2 are quantified, based on the product determined by HPLC analysis. It is worth noting here that formate is found to be the product of the electrocatalytic CO_2 reduction reaction. As the potential is shifted towards more cathodic side, the current density of the reaction significantly increases. Based on the potential-dependent HPLC data analysis, shown in **Figure S4** (SI), for example, at potentials of -0.434, -0.534, -0.634, -0.734 and -0.934 V vs. RHE, the amounts of formate obtained in in 3600 s are 0.01 mM, 0.025 mM 0.031 mM, 0.040 mM and 1.269 mM, respectively. Not surprisingly, the current density and the formation of formate are significantly increased by applying a more negative potential.

The electrochemical reduction of CO_2 is further quantified with Faradic efficiency (FE), which is determined using the following equation (Eq. 2):

$FE_{HCOO^-} = N \times F \times n_{HCOO} \times 100\ \% / Q_{Total}$ ---------- Eq.2

where F is the Faraday constant (96,485 C mol^{-1}); N is the number of electrons required to form the product, i.e., 2 for a formate molecule ($HCOO^-$); t is the electrolysis time; and Q is the quantity of electric charge (Q = J × t, where J is the current in ampere).[43]

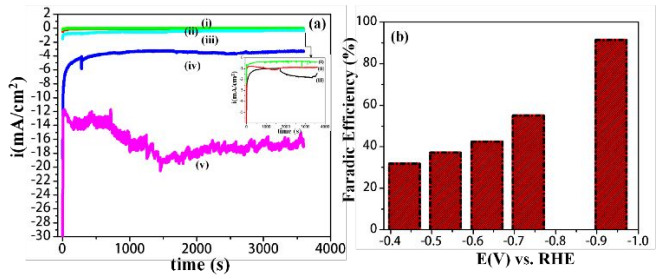

Figure 5. Bulk electrolysis performed for 3,600 s over (a) Al_2O_3-rGO at potentials of (i)-0.434 V, (ii) -0.534 V, (iii) -0.634 V, (iv) -0.734 V and (v) -0.934 V vs. RHE in $KHCO_3$ electrolyte bubbled with N_2 and then CO_2. (b) The values of FE obtained at applied potentials of -0.434, -0.534, -0.634, -0.734 and -0.934 V vs. RHE are found to be ~ 31.90, 37.25, 42.50, 55.10 and 91.20% , respectively. (The observed spikes in the current density is caused by the disturbances at the electrode/electrolyte interface due to CO_2 gas bubbles as well as and possible H_2 bubbles generated by the competitive reaction HER, which are common during experiments involving CO_2 reduction).

Bulk electrolysis is carried out over Al_2O_3-rGO in 0.5 M $KHCO_3$ saturated with CO_2 solution in the potential range of -0.434 V to -0.934 V vs. RHE, while CO_2 is continuously being bubbled into the electrolyte solution. The result, which is shown in **Figure 5a**, indicates that, as the applied potential is turned towards more negative values, the current as well as the amount of formate forming in the reaction increases. Importantly, three processes may simultaneously take place at the working electrode, namely: a) the generation of formate and its desorption into the supporting electrolyte, b) mass transfer of CO_2 from bulk to the electrode via diffusion and c) a competitive hydrogen evolution reaction (HER). Again, the adsorption of CO_2 at the active sites of Al_2O_3-rGO via diffusion from bulk, followed with desorption of formate, can take place continuously. From the observed curves, it can be said that the modified electrode is highly stable under all applied potentials (in the range of -0.434 V to -0.934 V vs. RHE). In the case of the applied potential -0.934 V vs. RHE, the observed fluctuations in current density could be because, at more negative potential, the rate of cathodic reactions is comparatively high (both CO_2 reduction and HER). Hence, the bubbles of H_2 forming, growing and desorbing due to HER, which can simultaneously take place at the electrode/solution interfaces, results in such fluctuations (**Figure 5a(iii)**).The results obtained for potential-dependent FE study is shown in **Figure 5b**. The values of FE at applied potentials of -0.434 V, -0.534 V, -0.634 V, -0.734 V and -0.934 V vs. RHE are found to be ~31.90, 37.25, 42.50, 55.10 and 91.20%, respectively. The data also show that, as the potential is shifted towards more negative values, the current density increases significantly. This could be due to the transfer of relatively more electrons at the electrified electrode-electrolyte interface of Al_2O_3-rGO.

The bulk electrolysis product at different specific potential (in the range of -0.434 V to -0.934 V vs. RHE) is confirmed by HPLC. For reference, a standard run is performed in the HPLC. The results are displayed in **Figure S4** in SI. A peak corresponding to formate product around 15.9 to 16.1 min is observed in the HPLC and confirmed based on a reference standered used. Furthermore, different amounts of formate are produced at different potentials, as can be seen in **Figure S4.**

To determine the performances of individual electrocatalysts towards formate formation, bulk electrolysis is carried out on rGO at an applied potential of -0.934 V vs. RHE under the saturated N_2 followed by CO_2 in 0.5 M $KHCO_3$ supporting electrolyte. Formate is produced with FE of 39% (see the i-t profile and efficiency graph in **Figure S5** in SI). The error bar of electrochemical results and data has been included in **Figure S6** in SI. Based on these results, the main portion of the product formed at Al_2O_3-rGO interface is formate and the remaining is due to HER.

Finally, the possible mechanism by which Al_2O_3-rGO electrocatalyzes CO_2 reduction with high performance and large value of FE toward formate product at lower overpotential is proposed. From TEM of the material, shown in **Figure 2** earlier, Al_2O_3 particles present on rGO have small quasi-spherical sizes with corners and edges, which are known to serve as active sites for catalysis. Al_2O_3-rGO has catalytically active Al_2O_3 sites with small sizes, and thus large density of sites to interact with CO_2 species. Their edges have high co-ordination sites and so better ways to bind CO_2 and electrochemically reduce it at the electrode's surfaces. For example, Mbah et al. discussed that various transition metals for electrochemical reduction of CO_2 and H_2S splitting reactions.[44] The surfaces and morphological modifications created on the materials due to calcination render the materials enhanced electrocatalytic performance and greater stability in the redox reactions. With this in mind, and using information from the literature detailed below, the electron transfer processes and the formation of intermediates and products over Al_2O_3-rGO are proposed as shown in **Scheme 2**.

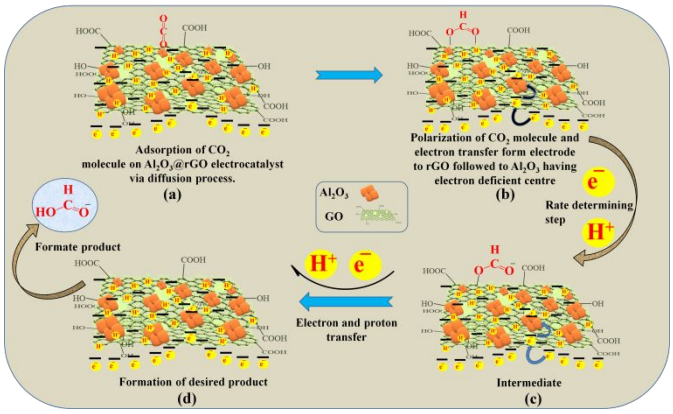

Scheme 2. Schematic representation of the possible reaction mechanism of CO_2 reduction over Al_2O_3-rGO producing formate.

Zuttel et al. reported on the electrochemical reduction of CO_2 over 3D indium oxide (In_2O_3) cathode that led to formate via electron transfer from electrode modified porous structure. This electrocatalyst gave only formate, indicating that the reaction proceeds via a two-electron transfer process and through CO intermediate. Again, the formate product formation has been governed by *OCHO intermediate during CO2 reduction reaction as concluded in theoretical insights studies whereas *COOH intermediate formation results in to for CO formation as a product. We thus believe that the same mechanism applies here as Al and In are in the same group and have stable +3 oxidation state and lower electronegativity than C.[45] In particular, the formation of *OCHO species as intermediate via O approaching from CO_2 towards the Al_2O_3-rGO electrocatalyst and which is possesses less energy for the product formation from intermediates is also analogous to the adsorption configuration of other transition metal ions like Sn and In.[46] Moreover, the literature indicates that Al enhances the kinetics related to electrochemical reduction of CO_2 rather than the HER due to its low affinity towards hydrogen whereas other metals such as Pd have a high affinity towards hydrogen and thus suppressing the CO_2 reduction.[47] In addition, Phania et al. reported on the electrocatalytic activity of B-doped graphene for reduction of CO_2 to formate.[48] Moreover, DFT calculations revealed that rGO and boron introduce more surface area with asymmetric charge density, which is responsible for CO_2 adsorption and subsequent conversion to formate.[48]

The highest adsorption energy reported for the formation of formate product via an electrochemical reduction of CO_2 is for boron-doped graphene, which has analogous structure to our Al_2O_3-rGO system.[48] Moreover, the performance of the present catalyst is compared with various reported electrocatalytic systems from the literature including carbon-supported Bi nanoparticles,[49] carbon black supported SnO_2,[50] and Sn-based gas diffusion electrode prepared by placing Sn on Nafion-bonded carbon black.[51] The data, which are summarized in **Table S1** in **SI**, indicate that Al_2O_3-rGO is a better electrocatalyst for CO_2 reduction than many reported systems. This could be due to the synergistic cooperative interactions between Al_2O_3 and rGO, since pure Al_2O_3 and rGO did not catalyze the reaction that well on their own.

Conclusions

We have demonstrated the synthesis of Al_2O_3-rGO via a simple chemical synthetic procedure that involved the preparation of rGO, followed by CVD of $AlCl_3$ into rGO an inert atmosphere. Structural and morphological characterization indicated the successful decoration of rGO with Al_2O_3 nanoparticles with 8±0.3 nm in size. The amount of Al in the material, as analyzed by ICP-MS analysis, was found to be ~2.8%. The material showed very good electrocatalytic activity toward the hydrogenation or reduction of CO_2, and its good catalytic activity was attributed to the synergetic effects between Al_2O_3 nanoparticles and underlying support material (i.e., rGO). The onset potential for the reaction was -0.434 V vs. RHE in aqueous $KHCO_3$ electrolytes. Additionally, potential-dependent bulk electrolysis showed that the reduction product was formate, which formed with a Faradaic efficiency (FE) of ~31.90, 37.25, 42.50, 55.10 and 91.20% at potentials of -0.434, -0.534, -0.634, -0.734 and -0.934 V vs. RHE, respectively. Neqiust plots showed that Al_2O_3-rGO had a good electron transport property. This material, which is composed of earth-abundant elements, could be viable for large-scale conversion of CO_2 into valuable products while helping reduce global warming.

Acknowledgements

Authors BBM and BDB are grateful to the University Grant Commission (UGC), New Delhi (India) for SRF Fellowship. BRS is thankful to CSIR HRDG project Sanction No: 01(2922)/18/EMR-II dated 11-10-2021, DST-SERB, New Delhi (India) for Research Project, Ref F.NO.SERB/F/7490/2016-17 and DAE-BRNS, Mumbai (India) for Research Project (Ref F. No. 34/20/06/2014-BRNS/21gs) for financial assistance. We are also thankful to the Chemistry Department at Dr. Babasaheb Ambedkar Marathwada University, Aurangabad-431004 (MS) India, for providing laboratory facilities to perform the research project. AVB acknowledges CSMCRI Bhavnagar and HCP0009 for providing the facility and financial assistance to perform some of the experiments included in the manuscript.

Notes and references

1 A. Buis, *Atmosphere*.,2019, **10**, 1-12.
2 S. Bilgen, *Renew. Sust. Energ. Rev.*,2014, **38**, 890-902.
3 Y. Tashiro, S. Hirano, M. M. Matson, S. Atsumi, A. Kondo, *Metab Eng.*,2018, **47**, 211-218.
4 M. Liu, Y. Yi, L. Wang, H. Guo, A. Bogaerts, *Catalysts*, 2019, **9**, 1-37.
5 B. Kumar, M. Llorente, J. Froehlich, T. Dang, A. Sathrum, P. C. Kubiak, *Annu. Rev. Phys. Chem*., 2012, **63**, 541-69.
6 N. Uemoto, M. Furukawa, I. Tateishi, H. Katsumata, S. Kaneco, *Chem. Eng*., 2019, **3**, 1-10.
7 W. Zhang, Y. Hu, L. Ma, G. Zhu, Y. Wang, X. Xue, R. Chen, S. Yang, Z. Jin, *Adv. Sci*., 2018, **5**, 1700275.
8 J. M. Barlow, J. Y. Yang, *ACS Cent. Sci*.,2019, **5**, 580-588.
9 Y. Hori, Modern Aspects of Electrochemistry, 2008, **42**. Springer, New York, NY, Online ISBN: 978-0-387-49489-0.
10 J. H. Zhou, Y. W. Zhang, *React. Chem. Eng*.,2018, **3**, 591-625.
11 S. Zhao, R. Jin, R. Jin, *ACS Energy Lett*.,2018, **3**, 452-462.
12 L. Hou, J. Yan, L. Takele, Y. Wang, X. Yan, Y. Gao, *Inorg. Chem. Front*., 2019, **6**, 3363-3380.
13 D. R. Naikwadi, S. Mehra, K. Ravi, A. Kumar, A. V. Biradar, *ACS Sustain. Chem. Eng.,* 2022*,* **10**,8526-8538*.*
14 M. Perez-Fortes, J. C. Schoneberger, A. Boulamanti, G. Harrison, E. Tzimas, *Int. J. Hydrog. Energy*.,2016, **41**, 16444-16462.
15 F. Yu, P. Wei, Y. Yang, Y. Chen, L. Guo, Z. Peng, *Nano Materials Sci*.,2019, **1**, 60-69.
16 J. L. White, A. B. Bocarsly, *J. Electrochem. Soc*.,2016, **163**, H410-H416.
17 Y. Chen, M. W. Kanan, *J. Am. Chem. Soc*.,2012, **134**, 1986-1989
18 S. A. Abbas, S. -H. Kim, H. Saleem, S. -H. Ahn, K. -D. Jung, *Catalysts*, 2019, **9**, 1-13.
19 G. Wen, D. Un Lee, B. Ren, F. M. Hassan, G. Jiang, Z. P. Cano,

J. Gostick, E. Croiset, Z. Bai, L. Yang, Z. Chen, *Adv. Energy Mater*., 2018, **8**, 1802427.
20 M. N. Mahmood, D. Masheder, C. J. Harty, *J. Appl. Electrochem.*, 1987, **17,** 1159-1170.
21 M. Hirata, T. Gotou, S. Horiuchi, M. Fujiwara, M. Ohba, *Carbon*, 2004, **42**, 2929-2937.
22 S. Navalon, A. Dhakshinamoorthy, M. Alvaro, H.Garcia, *Chem. Rev*., 2016, **312**, 99-148.
23 L. Feng, L. Wu, X. Qu, *Adv. Mat*., 2013, **25**, 168-186.
24 X. Yang, F. Zhang, L. Zhang, T. Zhang, Y. Huang, Y. A. Chen, *Adv. Funct. Mater*., 2013, **23**, 3353-3360.
25 T. Gan, S. Hu, *Microchim. Acta*., 2011, **175**, 1.
26 A. Ambrosi, C. K. Chua, N. M. Latiff, A. H. Loo, A. Wong, Y. A. HC. A. S. Eng, A. Bonanni, M. Pumera, *Chem. Soc. Rev*., 2016, **45**, 2458-2493.
27 G. M. Kim, Y. J. Park, Y. Shon, G. Shim, K. Y. Oh, *Curr. Pharm Biotechnol*., 2014, **14**, 1016-1026.
28 A. Pareek, S. J. Sravan, V. S. Mohan, *Materials Science for Energy Technologies*, 2019, **2**, 600-606.
29 C. Rogers, W. S. Perkins, G. Veber, E. T. Williams, R. R. Cloke, F. R. Fischer, *J. Am. Chem. Soc*., 2017, **139**, 4052-4061.
30 H. He, S. Sekoulopoulos, S. Zygmunt, *J. Phys. Chem. C*.,2016, **120**, 16732-16740
31 S. Zhang, P. Kang, T. J. Meyer, *J. Am. Chem. Soc*., 2014, **136**, 1734-1737.
32 K. Takahashi, K. Hashimoto, A. Fujishima, K. Omata, N. Kimura, *Chem. J. Chinese U*., 1994, **16**, 189-192.
33 S. Basu, A. Shegokar, D.Biswal, *J. CO_2 Util*.,2017, **18**, 80-88.
34 Y. E. Kim, W. Lee, M. H. Youn, S. K. Jeong, H. J.Kim, J. C.ParkK.T.Park, *J. Ind. Eng. Chem*.,2019, **78**, 73-78.
35 F. M. Segala, M. F. Correab, R. Bacanie, B. Castanheirac, M. J. Politid, S. Brochsztain, E. R. Tribonia, *Materials Research.*,2018, **21**, (1-8).
36 S. A. Ansari, Q. Husain, *J Mol Catal B-Enzym*., 2011, **70,** 119-126.
37 M. Ikram, Z. Tao, J. Ye, H. A. Qayyum, X. Suna, J. Xu, *RSC Adv*.,2018, **8**, 8329-8337.
38 J. A. Rotole, P. M. A. Sherwood, *Surface Science Spectra*.,1998, **5**, 18-24.
39 L. Zilberberg, H. Shankar, S. Mitlin, R. Elitsur, M. Asscher, *Langmuir*, 2018, **34**, 2610-2618.
40 P. K Nayak, J. A. Caraveo-Frescas, Z. Wang, *Sci. Rep*., 2014, **4**,4672.
41 B. B. Mulik, B. D. Bankar, A. V. Munde, A. V. Biradar, B. R. Sathe, *Chem. Eur. J.*,2020, **26**, 8801-8809.
42 Q. Wang, H. Dong, H. Yu, H. Yua, M. Liu, *RSC Adv*.,2015, **5**, 10346-10351.
43 B. B. Mulik, B. D. Bankar, A. V.Munde, P. P. Chavan, A. V. Biradar, B. R. Sathe, *Appl. Surf. Sci*.,2020, **538**, 148120.
44 N. O. Egiebor, J. Mbah, *Handbook of Climate Change Mitigation and Adaptatio*n, 2015, 1-19
45 X. An, S. Li, A. Yoshida, Z. Wang, X. Hao, A. Abudula, G. Guan, *ACS Sustainable Chem. Eng*., 2019, **7**, 9360-9368.
46 J. L. White, A. B. Bocarsly, *J. Electrochem. Soc.*,2016, **163,** H410-H416.
47 J. Qiao, Y. Liu, J. Zhang, *Boca Raton: CRC Press*, 2016, Routledge Handbooks Online.
48 N. Sreekanth, M. N. Azeezulla, T. V. Vineesha, K. Sailaja, K. L. Phani, *Chem. Commun*.,2015,**51**, 16061-16064.
49 B. Avila-Bolivar, L. García-Cruz, V. Montiel, J. Solla-Gullon, *Molecules*, 2019, **24**, 1-15.
50 H. Xiang, H. A. Miller, M. Bellini, H. Christensen, K. Scott, S. Rasula, H. E. Yu, *Sustain. Energ&Fuels*, 2020, **4**, 277-284.
51 Q. Wang, X. Wang, C. Wu, *Sci. Rep*., 2017**, 7,** 13711.